Unstable Air–Sea Interactions in the Tropics

S. G. H. PHILANDER

Geophysical Fluid Dynamics Laboratory/NOAA, Princeton University, Princeton, NJ 08542

T. YAMAGATA

Geophysical Fluid Dynamics Program, Princeton University, Princeton, NJ 08542

R. C. PACANOWSKI

Geophysical Fluid Dynamics Laboratory/NOAA, Princeton University, Princeton, NJ 08542

(Manuscript received 6 June 1983, in final form 1 November 1983)

ABSTRACT

During El Niño Southern Oscillation events modest anomalies amplify spatially and temporally until the entire tropical Pacific Ocean and the global atmospheric circulation are affected. Unstable interactions between the ocean and atmosphere could cause this amplification when the release of latent heat by the ocean affects the atmosphere in such a manner that the altered surface winds induce the further release of latent heat. Coupled shallow water models are used to simulate this instability which is modulated by the seasonal movements of the atmospheric convergence zones.

1. Introduction

The term El Niño refers to the interannual appearance of unusual oceanographic conditions—exceptionally high sea-surface temperatures, for example,—in the tropical Pacific. The term Southern Oscillation refers to interannual changes in the atmospheric pressure gradient across the tropical Pacific and, more generally, to other associated meteorological changes such as variations in the intensity of the trade winds. Bjerknes (1966) pointed out that El Niño and Southern Oscillation events coincide and that they are two aspects of the same phenomenon (ENSO). He suggested that the events are caused by interactions between the ocean and atmosphere. This idea has been dormant for nearly twenty years. During that time there has been enormous progress in our understanding of the response of the tropical oceans to specified changes in the surface winds, and in our understanding of the response of the atmosphere to heat sources in the tropics. The purpose of this paper is to reexamine the interactions between the tropical oceans and atmosphere in the light of these results and to propose that ENSO is indeed caused by interactions between the tropical Pacific Ocean and atmosphere.

During El Niño Southern Oscillation (ENSO) events, anomalous conditions in the ocean and atmosphere amplify simultaneously. In 1982 for example, modest anomalies that first appeared in the western tropical Pacific Ocean in May grew spatially and temporally until they reached a maximum amplitude in October (see Fig. 1). By that time intense westerly winds had penetrated into the central tropical Pacific Ocean, and sea surface temperatures in the central and eastern tropical Pacific were exceptionally high (Halpern *et al.*, 1983; Rasmusson and Wallace, 1983; Cane, 1983; Philander, 1983a,b). During the more common ENSO events, those of 1972 and 1976 for example, precursors with a modest amplitude appear in the western and eastern tropical Pacific in February and March. Six months later the anomalies have grown considerably, in amplitude and in areal extent so that the entire tropical Pacific is affected (Rasmussen and Carpenter, 1982). This simultaneous growth of anomalous conditions in the ocean and atmosphere suggests that air–sea interactions are of central importance in the answer to the key question, namely, What causes modest initial anomalies to amplify spatially and temporally during ENSO events?

Most studies of ENSO address two different questions: What is the response of the ocean to the changes in surface winds observed during ENSO? What is the response of the atmosphere to the high sea surface temperatures observed during ENSO? Though answers to these questions do not explain why ENSO occurs, they greatly enhance our understanding of these events. The oceanographic studies (Wyrtki, 1975; Hurlburt *et al.*, 1976; McCreary, 1976; Philander, 1981), reveal that the weakening of the trade winds during ENSO causes a horizontal redistribution of heat in the upper

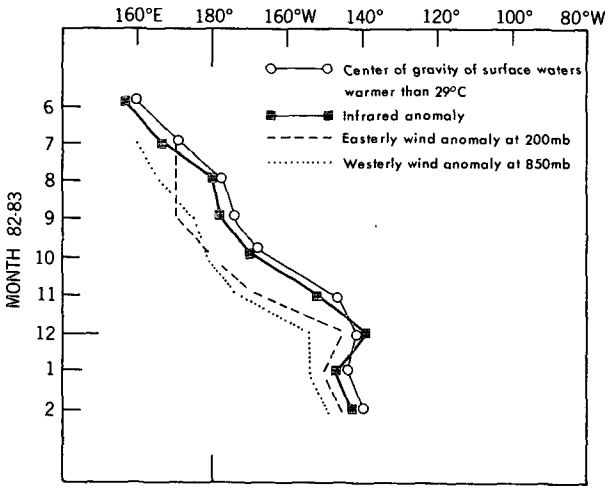

FIG. 1. The eastward expansion of anomalous conditions in the equatorial Pacific (5°N to 5°S) during 1982–83. The axes of the anomalous cloudiness, and winds are shown. (Courtesy of E. Rasmusson)

ocean and consequently causes the appearance of anomalously warm surface waters in the central and eastern tropical Pacific Ocean. Normally the westward trade winds maintain an eastward pressure force which is associated with isotherms that slope upwards towards the east. The isotherms become more horizontal when the westward winds weaken so that the eastern tropical Pacific becomes warmer. (In the western Pacific the thermocline rises but the sea-surface temperature remains unchanged because of the great depth of the thermocline in that region.) It is unnecessary for the winds over the entire basin to weaken for this redistribution of heat to occur. A weakening of the winds that is confined to only part of the equatorial ocean, the western Pacific say, can still result in a warming in the east because of eastward traveling oceanic Kelvin waves excited in the region where the winds weaken. In summary, the oceanographic results indicate that the relaxation of the trades causes the unusually high sea surface temperatures in the central and eastern equatorial Pacific during ENSO.

Meteorological studies suggest that the unusually high sea-surface temperatures cause the relaxation of the trades (Matsuno, 1966; Webster, 1972; Gill, 1980; Zebiak, 1982). If unusually warm surface waters in the central tropical Pacific Ocean cause a local heating of the atmosphere then the convergence of low level winds onto that region results in westerly wind anomalies over the western and central tropical Pacific.

Philander (1983a) points out that the oceanographic and meteorological results summarized here imply that unstable air–sea interactions are possible. This instability can cause modest anomalies to grow spatially and temporally in the following manner. Consider a pool of unusually warm surface waters that heats the atmosphere locally. The surface winds that converge on the heated region weaken the prevailing westward trade winds to the west of the pool but intensify them to the east of the pool. In the region of weakened winds the sea-surface temperatures increase for oceanographic reasons alluded to earlier and this, in turn, causes a further weakening of the winds. In this manner, the oceanic and atmospheric anomalies grow in amplitude. To the east of the original anomaly, matters are more complex because two factors determine the sea-surface temperature. One is the local intensification of the trades which increases equatorial upwelling and hence reduces the SST. The other is the weakening of the winds west of the anomaly which excites Kelvin waves that increase the SST east of the anomaly. Whether or not the warm surface waters expand eastward depends on which of the two factors is dominant.

In this paper, unstable air–sea interactions in the tropics are studied by means of a simple model that assumes that linear shallow water equations describe the oceanic and atmospheric motion. This model—details are given in Section 2—is of special interest in spite of its limited capability because its oceanographic and meteorological components have been widely (and separately) used to simulate variability in the tropical Pacific Ocean and in the tropical atmosphere. (See Busalacchi and O'Brien, 1981; Gill and Rasmusson, 1983; for example.) Section 3 of this paper describes unstable eigenvalues of the coupled model while Section 4 concerns the manner in which perturbations grow spatially and temporally. The relevance of these results to ENSO events, and the severe limitations of this model are discussed in Section 5.

2. The model

a. *The atmosphere*

Steady atmospheric motion in response to a heat source $Q(x, y, t)$ is described by the equations,

$$-fV + gH_x = -AU, \tag{1a}$$

$$fU + gH_y = -AV, \tag{1b}$$

$$D(U_x + V_y) = -BH - Q. \tag{1c}$$

The coordinates (x, y) measure distance in an eastward and northward direction; the corresponding velocity components are U and V. The one-layer atmosphere has an equivalent depth D. Perturbations to this depth are measured by H. The coefficient for Raleigh friction is A, and the coefficient for Newtonian cooling is B. The Coriolis parameter $f = \beta y$ vanishes at the equator ($y = 0$) and $C_a = (gD)^{1/2}$ is the long gravity wave speed.

Figure 2 depicts the atmospheric response to a heat source centered on the equator

$$Q = \exp[-(x^2 + y^2)/(500\ \text{km})^2]. \tag{2}$$

In these calculations $C_a = 66\ \text{m s}^{-1}$ so that the equatorial radius of deformation is 2000 km approximately.

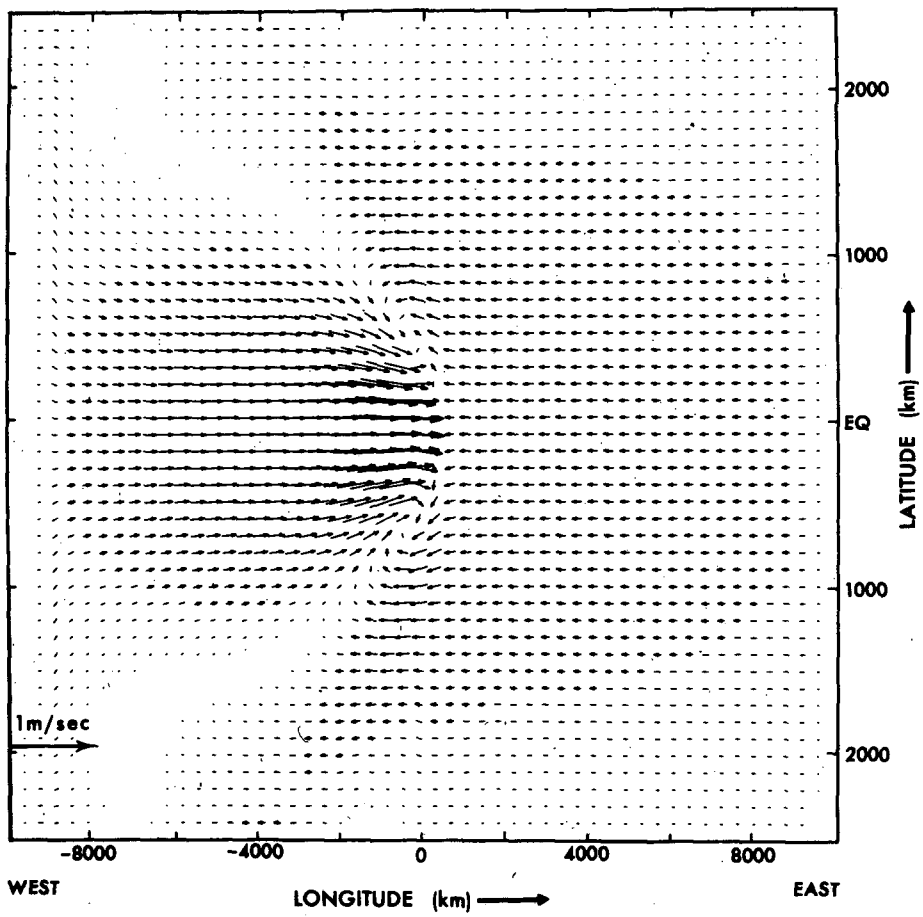

FIG. 2. The convergent flow induced by heating in the atmospheric model of Section 2.

Reduced gravity has the value 40 cm s^{-2} and the dissipation rates are

$$A = 1/5 \text{ days}, \quad B = 1/15 \text{ days}.$$

The solution in Fig. 2 has been discussed in detail by Matsuno (1966), Webster (1972), Gill (1980) and Zebiak (1982).

b. The ocean

Oceanic motion in response to a body-force (τ^x, τ^y) is described by the equations

$$u_t - f_v + gh_x = -au + \tau^x, \tag{3a}$$

$$v_t + fu + gh_y = -av + \tau^y, \tag{3b}$$

$$h_t + d(u_x + v_y) = -bh. \tag{3c}$$

The zonal (u) and meridional (v) velocity components in an ocean with equivalent depth d are associated with depth perturbations h. Motion is damped by Raleigh friction (coefficient a) and Newtonian cooling (coefficient b). The long gravity wave speed is $C_o = (gd)^{1/2}$, and reduced gravity has the value 2 cm s^{-2}.

Figure 3 shows the dispersion of an initial perturbation in the height field

$$h = 0.2 \exp[-(x^2 + y^2)/(500 \text{ km})^2] \text{ cm} \tag{4}$$

that is maintained for 10 days. In these calculations $a = 1/100$ days, $b = 1/100$ days and $C_o = 140$ cm s^{-1} so that the equatorial radius of deformation is 250 km and the equatorial inertial time $(1/\beta c)^{1/2}$ is 1.5 days. The perturbation is seen to disperse into westward traveling Rossby waves and an eastward propagating Kelvin wave. (For details of the numerical method used to obtain these solutions see Appendix.) The value assigned to the equivalent depth (h = 20 cm) is the appropriate one if the sharp, shallow tropical thermocline is regarded as an interface between the warm surface waters and the cold deep water of the ocean.

c. Coupling between the ocean and atmosphere

The simplest, though by no means most realistic, manner in which to couple the ocean and atmosphere is to assume that changes in the depth of the thermocline h affect the sea–surface temperature which, in turn, heats (or cools) the atmosphere.

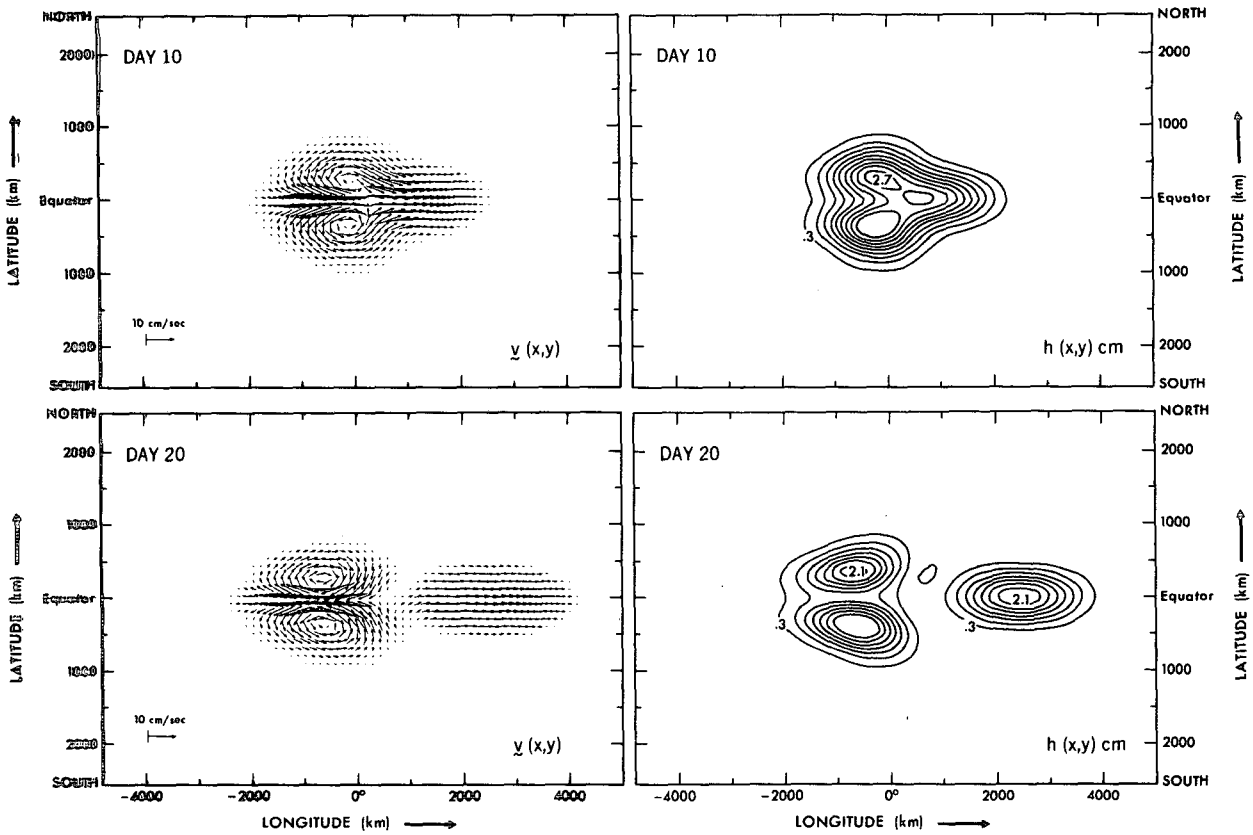

FIG. 3. Dispersion of perturbation in the depth of the thermocline.

$$Q = \alpha h. \tag{5a}$$

Atmospheric winds are assumed to act as a body force in the ocean,

$$(\tau^x, \tau^y) = \gamma(U, V). \tag{5b}$$

Approximate numerical values for the interaction coefficients α and γ can be obtained as follows. Assume that a change in sea-surface temperature ΔT is linearly related to a change in thermocline depth and that ΔT is 1 K for a 50 m decrease in the depth of the thermocline (or a 10 cm decrease in equivalent depth h). The Clausius–Clapeyron equation can then be used to relate ΔT to the heat released to the atmosphere if it is assumed that the air is always saturated by the water vapor supplied by the ocean. For an average sea surface temperature of 300 K and for approximate time of latent heat release of 1 day, it can be shown that

$$\alpha = 10^{-2}\ \text{s}^{-1}. \tag{6a}$$

This is also the appropriate value if a thermocline depression of 10 m (or a change in h of 2 cm) causes heating of the atmosphere that is associated with convergence of (23 days)$^{-1}$.

To estimate γ assume that a steady wind of 2 m s^{-1} that persists for 10 days accelerates an equatorial jet to 1 m s^{-1}. Then

$$\gamma = 5 \times 10^{-7}\ \text{s}^{-1}. \tag{6b}$$

The values for α and γ in Eq. (6a,b) are only approximate estimates so that the sensitivity of the results to changes in the values of α and γ will be discussed later. Note that the oceanic motion is unaffected by changes in the values of α and γ that leave the product $\alpha\gamma$ unchanged. [This can readily be inferred from Eqs. (1), (3) and (5).]

This model has a number of flaws. For example, the loss of heat by the ocean leaves the ocean unaffected and an increase in sea-surface temperature (thermocline depth) necessarily causes heating of the atmosphere. These unrealistic features, especially the latter one, are discussed in Section 5.

3. Unstable modes

a. Nonrotating case

Assume that neither the ocean nor atmosphere is rotating. Assume furthermore that $A = B$ and $a = b$. In that case, solutions of the following form are possible

$$(u, v, h, U, V, H) = (u, v, h, U, V, H)e^{i(kx+ly-\sigma t)}, \quad (7)$$

provided

$$(-i\sigma + a)^2 = C_o^2(\mathcal{K}_c^2 - \mathcal{K}^2), \quad (8)$$

where

$$\left.\begin{aligned} \mathcal{K}^2 &= k^2 + l^2 \\ \mathcal{K}_c^2 &= \frac{\alpha\gamma - A^2}{C_a^2} \end{aligned}\right\}.$$

In the absence of dissipation ($A = a = 0$) disturbances with wavenumber $\mathcal{K} < \mathcal{K}_c$ are unstable and grow exponentially. Short waves ($\mathcal{K} > \mathcal{K}_c$), on the other hand, are stable. The physical reason for this is the following. An initial perturbation, a depression of the thermocline for example causes a heating of the atmosphere. The air that converges on the depression also drives convergent motion in the ocean so that the depression tends to grow. However, the gravitational restoring force associated with the stratification of the ocean tends to eliminate the original depression. This restoring force increases as the horizontal scale of the depression decreases. In the case of disturbances with a small horizontal scale ($\mathcal{K} > \mathcal{K}_c$) the gravitational restoring force in the ocean is dominant but for large horizontal scales ($\mathcal{K} < \mathcal{K}_c$) the initial perturbation is unstable.

b. Constant rotation

In the case where the Coriolis parameter has a constant value the counterpart to Eq. (8) is

$$(-i\sigma + a)^3 + p(-i\sigma + a) + q = 0, \quad (9)$$

where

$$\left.\begin{aligned} p &= C_a\mathcal{K}^2 + f^2 - \frac{\alpha\gamma C_o^2\mathcal{K}^2}{C_a^2\mathcal{K}^2 + f^2 + A^2} \\ q &= \frac{\alpha\gamma C_o^2\mathcal{K}^2 f^2}{A(C_a^2\mathcal{K}^2 + f^2 + A^2)} \end{aligned}\right\}.$$

At high frequencies $\sigma \gg f$ the effects of rotation are unimportant and the earlier results are recovered. At low frequencies ($\sigma < f$), however, Eq. (9) does not appear to have any unstable modes. The reason is the following. From Eqs. 1(a), (b), 3(a), (b) and 5(b) it can be inferred that on time-scales long compared to an inertial period

$$\mathrm{div}(u, v) = -\frac{\alpha}{A}\,\mathrm{div}(U, V), \quad (10)$$

provided the oceanic dissipation time $1/a$ is long compared to an inertial period. In other words, convergent motion in the atmosphere drives divergent motion in the ocean. (In a more sophisticated model that has Ekman layers it can readily be shown that the surface wind convergence is equal to the divergence of the currents in the upper ocean.) This result rules out the instabilities that require convergent winds to drive convergent oceanic currents.

c. The equatorial β-plane

On an equatorial β-plane Eq. (10) is invalid and it is possible for convergent surface winds to drive convergent motion in the ocean. Instabilities should therefore be possible near the equator. (The equatorial β-plane has some of the properties of the nonrotating case discussed earlier because the Coriolis parameter vanishes at the equator.) Lau (1981) demonstrated that in a coupled ocean–atmosphere system equatorial Kelvin waves are unstable. His model, however, is restricted because it permits meridional motion in neither the ocean nor atmosphere. A more consistent model, described in Section 2, permits an analytical stability analysis only if $C_a = C_o$ so that the ocean and atmosphere have the same radius of deformation. Though the assumption $C_a = C_o$ is indefensible it is reassuring that this case has unstable modes such as those in Fig. 4. The results in Fig. 4 were obtained by describing the oceanic and atmospheric variables in terms of Hermite Functions H_n. For example

$$v = \sum v_n H_n e^{(ikx-\sigma t)}; \quad V = \sum V_n H_n e^{i(kx-\sigma t)}.$$

Truncation of this series at $n = 2$ results in an algebraic equation for σ. The main result is that large-scale low-frequency unstable modes do exist.

Zebiak (personal communication, 1983) explored the limit $C_o \ll C_a$ and also finds unstable modes.

The general case where C_o and C_a have arbitrary values is beyond the scope of this paper. A more complete stability analysis of this problem will be presented on another occasion.

4. Spatially and temporally growing perturbations

To study the spatial and temporal growth of an initial perturbation, we use the numerical methods described in the Appendix. The perturbation is a depression of the thermocline with a Gaussian shape [Eq. (4)] that is maintained for 10 days whereafter motion is driven by the interaction between the ocean and atmosphere. Fig. 5 shows how these interactions cause oceanic and atmospheric fields to amplify. (Calculations are terminated when the perturbations to the mean depth of the ocean have the same amplitude and opposite sign as the mean depth.) The depression of the thermocline is seen to expand westward because the westerly winds to the west of the heat source drive convergent oceanic motion and an eastward equatorial jet. Initially, the deepening of the equatorial thermocline in the western part of the basin is at the expense of the extra-equatorial thermocline which rises. The eastward oceanic jet soon causes the thermocline in the far west to rise and this sustains the growth of the initial perturbation (Fig. 6). The amplification of the

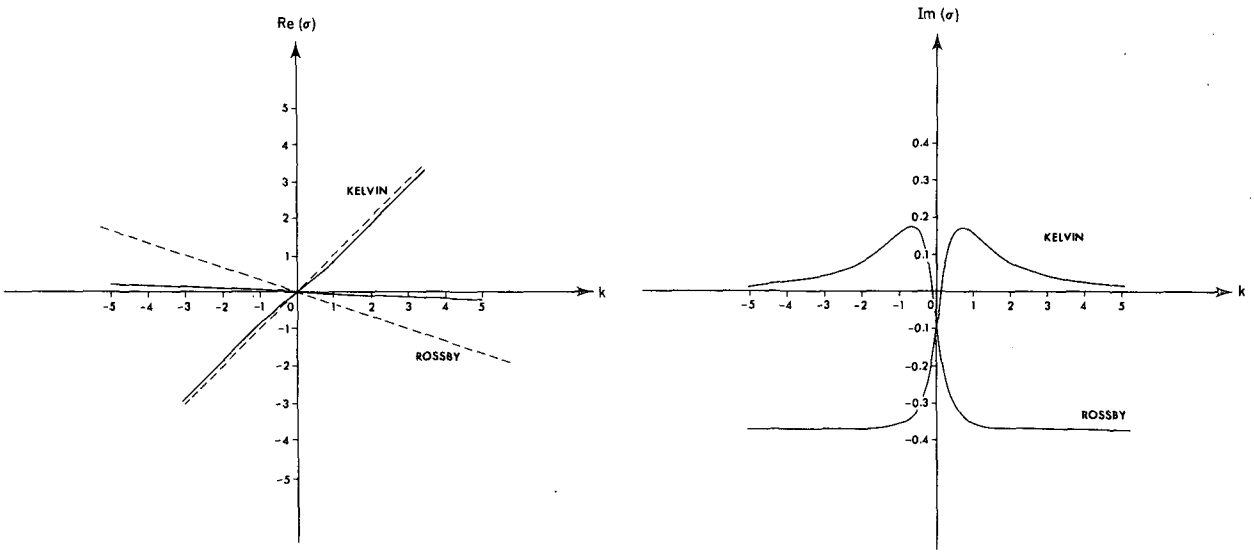

FIG. 4. The dispersion diagram for unstable modes on an equatorial β-plane when $C_a = C_o = C$. The unit of distance is the radius of deformation $\lambda = (C/2\beta)^{1/2}$; the unit of time is $T = (2\beta C)^{-1/2}$. The dashed line is the dispersion curve in the absence of air–sea interaction. These results are for parameter values $a = b = 0$, $A = B = -3/T$ and $\alpha\gamma = 0.3/T^2$.

oceanographic and meteorological fields to the west of the initial perturbation is not a gradual westward expansion as in Rasmusson and Carpenter's (1982) description of a typical El Niño, but is rather a very rapid westward expansion within the first few days, followed by a gradual *in situ* amplification in the western part of the basin. (Numerical experiments in which the initial perturbation is adjacent to the eastern coast of the ocean basin gave essentially the same results.) The difference between the model and the measurements can in part be attributed to different reference states. In the model the perturbations are relative to a background state which is a state of no motion. Rasmusson and Carpenter (1982) describe the evolution of El Niño anomalies relative to a background state which corresponds to climatological conditions. The climatology is a function of space and time. For example the annual harmonic of sea surface temperature (SST) has westward phase propagation (Horel, 1982). During a typical El Niño, SST anomalies (relative to the climatology) gradually expand westward but there is no westward phase propagation evident in the actual SST field. The SST is exceptionally high during the early stages of El Niño and these warm conditions then persist for several months. (In other words, the seasonal decrease in SST, which is characterized by westward phase propagation,

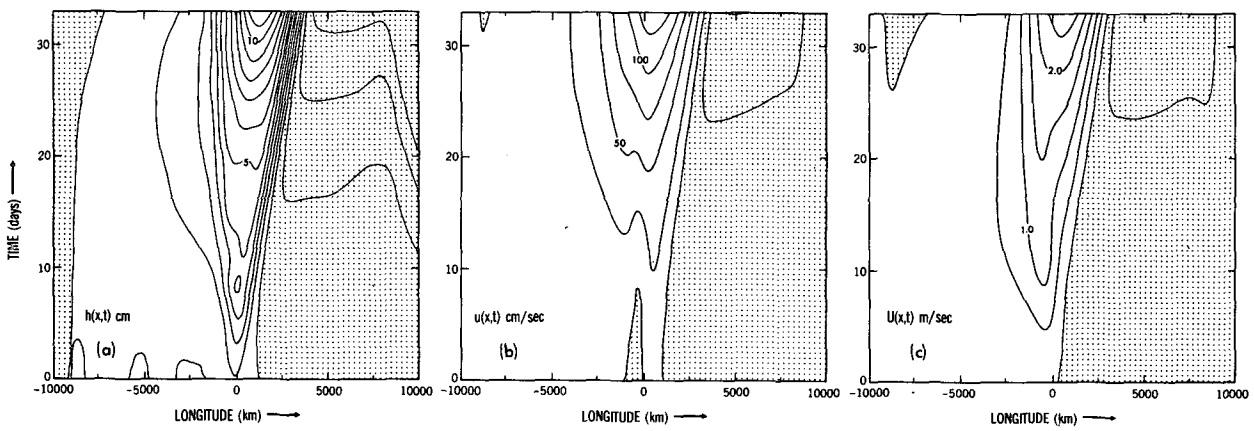

FIG. 5. Perturbation to the depth of the thermocline (a) and the zonal currents in the ocean (b) and atmosphere (c) as a function of longitude and time in the coupled models. Motion is westward and the thermocline is elevated in shaded region. In these calculations C_a = 66 m s^{-1}, C_o = 1.4 m s^{-1}, $\alpha = 10^{-2}$ s^{-1} and $\gamma = 0.5 \times 10^{-6}$ s^{-1}. The dissipation parameters have the values given in Section 2.

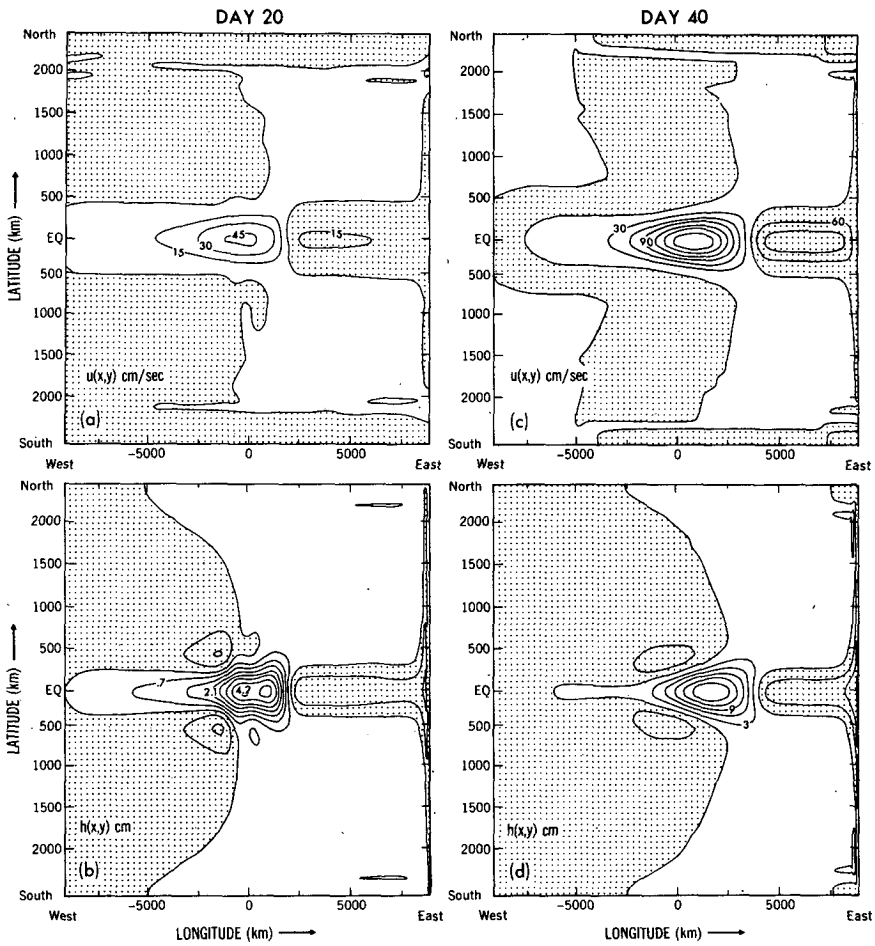

FIG. 6. Spatial structure of the zonal velocity component and of the depth of the thermocline after 20 [in (a) and (b)] and 40 days [in (c) and (d)]. Motion is westward and the thermocline is elevated in shaded regions. Parameter values as for Fig. 5.

fails to materialize during El Niño.) To compare the model in detail with the measurements, it will be necessary to include the seasonal cycle in the model.

To the east of the initial perturbation, weak easterly winds elevate the thermocline and drive a westward oceanic current. Fig. 5 shows that these conditions gradually recede eastward as the original perturbation expands in that direction. The speed of this expansion is approximately the oceanic Kelvin wave speed and is in good agreement with the evolution of the 1982–83 event (Fig. 1). This is consistent with the results of Fig. 4 according to which the group velocity of the unstable modes is practically the same as that of the stable modes. (Keep in mind however that the results of Fig. 4 are based on the unrealistic assumption $C_o = C_a$.)

The deepening of the thermocline expands eastward because the upwelling induced in the eastern side of the basin by the easterly winds is overwhelmed by the downwelling caused by Kelvin waves excited by the westerly winds over the western side of the basin. This result is in part a consequence of the asymmetric response of the atmosphere to a heat source. In Fig. 2, for example, the westerly winds in the west are more intense than the easterly winds in the east. To explore the sensitivity of the air–sea interactions to this asymmetry, the ocean was coupled to an atmosphere in which the easterlies and westerlies are of equal intensity in response to the heating function of Eq. (2). This is accomplished by making the atmosphere nonrotating so that there is axisymmetric convergence over the heated region. This would be the case if the dimensions of the heated zone were very small compared to the radius of deformation of the atmosphere. Fig. 7 shows the results. The easterly winds and the elevation of the thermocline to the east of the original perturbation is more intense than before, and the eastward expansion of the deepening of the thermocline is much more gradual. The conclusion is that the response to the east of the original perturbation is sensitive to the details

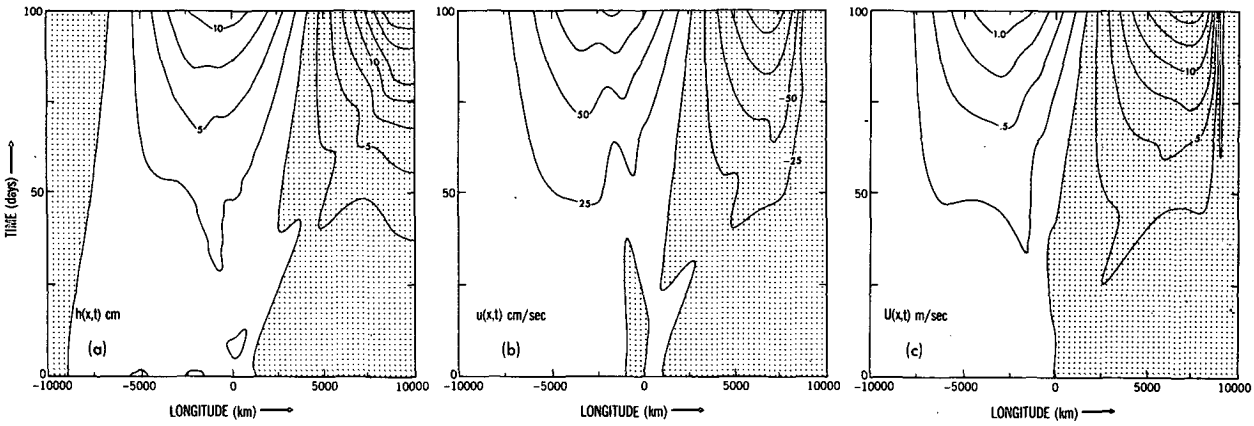

FIG. 7. As in Fig. 5 but the ocean is coupled to a nonrotating atmosphere.

of the atmospheric winds induced by the heating function.

In Sections 2 and 3 we noted that the unstable air–sea interactions depend on the product $\alpha\gamma$. The values assigned to these parameters in Section 2 are approximate estimates. Fig. 8 shows how changes in the value of $\alpha\gamma$ affect the *e*-folding time (as measured by the time it takes for the thermocline perturbations to amplify from 2 to 20 cm). The initial perturbation, as pointed out in Section 3, is subject to two opposing tendencies: gravitational restoring forces which favor dispersion and ocean–atmosphere interactions which favor amplification. When the value of $\alpha\gamma$ is 10^{-10} s^{-2} or less, then the effect of the wind on the ocean is negligible compared to the dispersive effect and the initial perturbation behaves as in Fig. 3. In Fig. 5, where $\alpha\gamma = 5 \times 10^{-9}$ s^{-2} amplification occurs but note that dispersive effects are still evident, in the tongue of westward flow near $x = 0$, $t = 0$ in Fig. 5(b) for example. In Fig. 7, where amplification rates are smaller than in Fig. 5, this tongue is more pronounced and there is also evidence of eastward dispersion into Kelvin waves.

Calculations in which the initial perturbation corresponds to weak eastward winds over a 500 km wide region in the center of the basin, maintained for 10 days, gave results essentially the same as those described here.

5. Discussion

Unstable air–sea interactions in the tropics can permit modest initial anomalies to grow temporally and spatially. This is the principal result of these calculations. Because of the crudeness of the model it would be an error to attach great significance to the details of the solutions (some of which are unrealistic, as pointed out in Fig. 4). The growth-rate for example is determined by the interactions between the ocean and atmosphere which have been parameterized in a simple but questionable manner. The assumption that anomalously high sea–surface temperatures always cause a local heating of the atmosphere is unrealistic. In reality unusually warm surface waters release an exceptional amount of water vapor to the atmosphere but the heating of the atmosphere is not necessarily local. It occurs where the water vapor rises and condenses. There is a local heating of the atmosphere over the warm anomaly only if there is rising air over the anomaly. This means that the movement of the large-scale atmospheric convergence zones will control the amplification of an initial perturbation. Philander (1983a) invoked this argument to explain the close relation between the seasonal cycle and the evolution of ENSO. Anomalous conditions in the western tropical Pacific

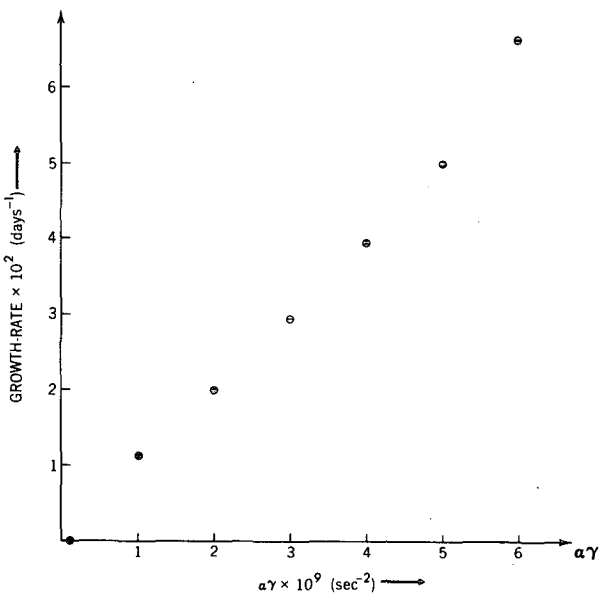

FIG. 8. Growth rates of unstable air–sea interactions as a function of $\alpha\gamma$. Other parameters have the same values as in Fig. 5.

Ocean, for example, are most likely to expand eastward in May or in September. Because of its seasonal meridional migrations the ascending branch of the Walker Cell is at the equator at those times. Anomalous conditions off the coast of Peru and Ecuador expand westward in February and March because that is when the ITCZ is close to the equator in the eastern Pacific. In the eastern tropical Atlantic Ocean the ITCZ does not move as far south seasonally as it does in the Pacific (Oort, 1982) so that ENSO-like events occur less frequently there. According to this view ENSO is an unstable air–sea interaction modulated by the seasonal cycle. It would therefore improve the model of Section 2 if the coefficient α in equation (5) were a function of space and time that describes the seasonal movements of the atmospheric convergence zones.

$$\alpha = \begin{cases} \alpha_0 \operatorname{div}(\bar{U} + U), & \text{if} \quad \operatorname{div}(\bar{U} + U) > 0 \\ 0, & \text{if} \quad \operatorname{div}(\bar{U} + U) < 0, \end{cases} \quad (11)$$

where α_0 is a constant, $\bar{U}$ denotes the mean atmospheric winds and U the anomalous winds. Initially when the perturbations have a small amplitude their growth is entirely controlled by the large-scale convergence field ($\operatorname{div}\bar{U}$) so that ENSO during its early stages is an amplification of the seasonal cycle. Once anomalous conditions have attained a large amplitude ($\operatorname{div}U \sim \operatorname{div}\bar{U}$) then the exceptionally warm surface waters can induce conditions favorable for their further growth. In the eastern Pacific ENSO resembles the seasonal cycle only during the early stages. Once anomalous conditions have expanded into the region west of 130°W, they continue to amplify but the seasonal cycle attenuates in that region (Horel, 1982). The seasonal cycle modulates the growth of ENSO even during its mature phase (Ramage and Hori, 1981) which implies that the term $\operatorname{div}\bar{U}$ in (11) is never negligible. This term, which describes the seasonal movements of the convergence zones, is determined by many factors; the sea surface temperature is only one. This means that factors outside the tropical Pacific exert a strong influence on ENSO. For example, ENSO often terminates while the central tropical Pacific Ocean is still anomalously warm. In 1983 easterly wind returned to the tropical Pacific west of the dateline in January and February even though the central Pacific continued to be exceptionally warm for several more months (Rasmusson and Wallace, 1983). Until the movements of the large-scale atmospheric convergence zones can be predicted, it will be difficult to predict ENSO. In 1975 anomalous conditions off the coast of Peru and Ecuador started to amplify but stopped doing so after a few weeks (Wyrtki *et al.*, 1976). It is conceivable that extratropical conditions caused a rapid poleward movement of the ITCZ and thus terminated the unstable air–sea interactions. In 1979 there were ENSO-like conditions over the western Pacific but these conditions did not expand eastward (Donguy *et al.*, 1982). In 1982 they did. A comparison of the atmospheric data that describes these events will be of considerable interest.

In the oceanic model of Section 2b it is assumed that the sea-surface temperature is a simple function of the depth of the thermocline. In reality the sea-surface temperature is strongly influenced by advection so that sea-surface temperature gradients are important. These gradients are largest in the eastern equatorial Pacific and very small in the western tropical Pacific Ocean, the warmest part of the Pacific. This means that the initial perturbation in the western Pacific is more likely to be anomalous westerly winds than anomalously warm surface waters. Because of the small sea surface temperature gradients in that region the winds would have to penetrate far east before there is a local positive feedback. This could explain why so few ENSO events expand eastward. Most events expand westward from the coast of Peru and Ecuador where sea-surface temperature gradients are large (Rasmusson and Carpenter 1982). These considerations suggest that the oceanographic model of Section 2 can be improved by specifying the observed sea-surface temperature gradients and by letting the currents in the model advect these gradients. Unfortunately, the shallow water model does not simulate the highly nonlinear equatorial currents in a realistic manner—there is no Equatorial Undercurrent in the model for example. It would be preferable to use a multilevel nonlinear model which is also capable of taking diabatic processes into account. The importance of these processes can be estimated by calculating the heat lost by the ocean during ENSO events. The excess precipitation over a large part of the tropical Pacific Ocean during ENSO is of the order of 0.3 cm per day for several months (Rasmusson and Carpenter, 1982). This means that over a period of 150 days the upper 100 m of the ocean is cooled 3°C! This figure is unrealistically large because it assumes that the evaporation occurs over the same area as the precipitation. The area over which evaporation takes place is of course larger but the heat lost by the ocean during ENSO is nonetheless considerable. It could be one of the factors that determine the termination of ENSO.

APPENDIX A

Equations (1) and (3) are solved numerically by finite difference methods after (1) has been modified to include the acceleration terms. The differencing scheme is the potential enstrophy conserving one of Sadourny (1975). The oceanic domain, a closed box, extends from 25°S to 25°N and has a longitudinal extent of 190°. The atmospheric domain is larger in the zonal direction by 20°. Diffusive regions in which the values

of A and B increase by a factor of 40 are added on each side of the ocean basin in order to prevent reflections. The adequacy of these diffusive regions was tested by doubling their longitudinal extent. This did not affect the results. The atmosphere in effect is zonally unbounded. Increased mixing within 5° latitude of the zonal coasts of the ocean damps coastal Kelvin waves. At all coasts, velocity components normal to that coast are specified to vanish. The grid spacing is 1° in the latitudinal and longitudinal directions in the ocean and atmosphere. The coupling between the ocean and atmosphere comes into effect once a day. For the rest of a day the driving forces for the ocean and atmosphere are held fixed.

REFERENCES

Bjerknes, J., 1966: A possible response of the atmospheric Hadley circulation to equatorial anomalies of ocean temperature. *Tellus,* **18,** 820–829.

Busalacchi, A., and J. J. O'Brien, 1981: Interannual variability of the equatorial Pacific in the 1960's. *J. Geophys. Res.* **86,** 10 901–10 907.

Cane, M., 1983: Oceanographic events during El Niño. *Science,* **222,** 1189–1195.

Donguy, J. R., C. Henin, A. Morliere, J. P. Rebert and G. Meyers, 1982: Appearances in the western Pacific of phenomena induced by El Niño. (unpublished manuscript).

Gill, A. E., 1980: Some simple solutions for heat-induced tropical circulation. *Quart. J. Roy. Meteor. Soc.,* **106,** 447–462.

——, and E. Rasmusson, 1983: The 1982–83 climate anomaly in the equatorial Pacific. *Nature,* **306,** 229–234.

Halpern, D., S. Hayes, A. Leetmaa, D. Hansen and G. Philander, 1983: Oceanographic observations of the 1982 warming of the tropical Pacific. *Science,* **221,** 1173–1175.

Horel, J. D., 1982: The annual cycle in the tropical Pacific atmosphere and ocean. *Mon. Wea. Rev.,* **110,** 1863–1878.

Hurlburt, H. E., J. C. Kindle and J. J. O'Brien, 1976: A numerical simulation of the onset of El Niño. *J. Phys. Oceanogr.,* **6,** 621–631.

Lau, K-M., 1981: Oscillations in a simple equatorial climate system. *J. Atmos. Sci.,* **38,** 248–261.

Matsuno, T., 1966: Quasi-geostrophic motions in equatorial areas. *J. Meteor. Soc. Japan,* **2,** 25–43.

McCreary, J., 1976: Eastern tropical ocean response to changing wind systems: With application to El Niño. *J. Phys. Oceanogr.,* **6,** 632–645.

Oort, A. H., 1983: Global Atmospheric Circulation Statistics 1958–1973. NOAA Prof. Pap. No. 14, Government Printing Office, Washington, DC, 180 pp.

Philander, S. G. H., 1981: The response of equatorial oceans to a relaxation of the trade winds. *J. Phys. Oceanogr.,* **11,** 176–189.

——, 1983a: El Niño Southern Oscillation phenomena. *Nature,* **302,** 245–301.

——, 1983b: Anomalous El Niño of 1982–83. *Nature,* **305,** 16.

Ramage, C. S., and A. M. Hori, 1981: Meteorological aspects of El Niño. *Mon. Wea. Rev.,* **109,** 1827–1835.

Rasmusson, E. M., and T. H. Carpenter, 1982: Variations in tropical sea surface temperature and surface wind fields associated with the Southern Oscillation/El Niño. *Mon. Wea. Rev.,* **110,** 354–384.

——, and J. M. Wallace, 1983: Meteorological aspects of the El Niño–Southern Oscillation. *Science,* **222,** 1195–1202.

Sadourny, R., 1975: The dynamics of finite difference models of the shallow water equations. *J. Atmos. Sci.,* **32,** 680–689.

Webster, P. J., 1972: Response of the tropical atmosphere to local steady forcing. *Mon. Wea. Rev.,* **100,** 518–541.

Wyrtki, K., 1975: El Niño—The dynamic response of the equatorial Pacific Ocean to atmospheric forcing. *J. Phys. Oceanogr.,* **5,** 572–584.

——, E. Stroup, W. Patzert, R. Williams and W. Quinn, 1976: Predicting and observing El Niño. *Science,* **191,** 343–346.

Zebiak, S. E., 1982: A simple atmospheric model of relevance to El Niño. *J. Atmos. Sci.,* **39,** 2017–2027.